Title	**Breakup dynamics and dripping-to-jetting transition in a Newtonian/shear-thinning multiphase microsystem**
Author(s)	**Ren, Y; Liu, Z; Shum, HC**
Citation	**Lab on a Chip, 2015, v. 15 n. 1, p. 121-134**
Issued Date	**2015**
URL	**http://hdl.handle.net/10722/217078**
Rights	**Creative Commons: Attribution 3.0 Hong Kong License**

Breakup dynamics and dripping-to-jetting transition in a Newtonian/shear-thinning multiphase microsystem

Yong Ren*[ab], Zhou Liu[ac] and Ho Cheung Shum*[ac]

[a]*Department of Mechanical Engineering, The University of Hong Kong, Pokfulam Road, Hong Kong.*

[b]*Current Address: Department of Mechanical, Materials & Manufacturing Engineering, The University of Nottingham, Ningbo, China.*

[c]*HKU-Shenzhen Institute of Research and Innovation (HKU-SIRI), Shenzhen, Guangdong, China.*

Author to whom correspondence should be addressed. E-mail: yong.ren@nottingham.edu.cn; ashum@hku.hk; Tel: +852 2859 7904

The breakup dynamics in non-Newtonian multiphase microsystems are associated with a variety of industrial applications such as food production and biomedical engineering. In this study, we numerically and experimentally characterize the dripping-to-jetting transition under various flow conditions in a Newtonian/shear-thinning multiphase microsystem. Our work can help to predict the formation of undesirable satellite droplet, which is one of the challenges in dispensing non-Newtonian fluids. We also demonstrate the variations in breakup dynamics between shear-thinning and Newtonian fluids under the same flow conditions. For shear-thinning fluids, droplet size increases when the Capillary number is smaller than a critical value, while decreases when Capillary number is beyond the critical value. The variations highlight the importance of rheological effects in flows with a non-Newtonian fluid. The viscosity of shear-thinning fluids significantly affects the control over droplet size, therefore necessitating the manipulation of the

24 shear rate through adjusting the flow rate and the dimension of the nozzle. Consequently, the

25 droplet size can be tuned in controlled manner. Our findings can guide the design of novel

26 microdevices for generating droplets of shear-thinning fluids with predetermined droplet

27 size.This enhances the ability to fabricate functional particles using an emulsion-templated

28 approach. Moreover, elastic effects are also investigated experimentally using a model shear-

29 thinning fluid that also exhibits elastic behaviors: droplets are increasingly deformed with

30 increasing elasticity of the continuous phase. The overall understanding in the model multiphase

31 microsystem will facilitate the use of a droplet-based approach for non-Newtonian multiphase

32 applications ranging from energy to biomedical sciences.

33 # 1. Introduction

34 Microfluidic multiphase system can be applied in a wide variety of applications. For example, it

35 can facilitate drug encapsulation and release using emulsion droplets as a template to fabricate

36 core-shell microspheres, capsules and other functional materials.[1-3]The system can also be used

37 for the generation of jets, which can work as precursors of microfibers for application in wound

38 dressing and tissue engineering.[2,4-7]Nevertheless, the practical microfluidic multiphase

39 applications increasingly demand the use of fluids with more complex rheological behaviors,

40 such as non-Newtonian fluids, whose viscosities change with the applied stress. Non-Newtonian

41 fluids are ubiquitous in daily life; examples include blood, lotions, creams, shampoos and

42 toothpaste. They are also widely used in industrial applications such as inkjet printing, spraying

43 and coating.[8-9]Microscaled non-Newtonian multiphase systems have been increasingly applied in

44 biomedical engineering, food production, and energy applications. For instance, an electrokinetic

45 microdevice has been developed to convert fluidic mechanical energy to electrical energy by

46 means of electrokinetic phenomena such as streaming currents.[9] By reducing the hydrodynamic

47 conductance while maintaining the same streaming current, addition of an appropriate polymer

48 to the working fluid in a microchannel can enhance the energy conversion efficiency, which is a

49 ratio of electrical output power and hydrodynamic input power.[10-11]

50 Non-Newtonian multiphase microsystem has become a subject of intense research, and it is of

51 paramount importance to understand the relevant physical phenomena, one of which involves the

52 deformation of liquid threads and subsequently droplet formation. The performance of the

53 droplets is intimately tied to the ability to control droplet size, which has a strong impact on the

54 droplet stability as well as optical and mechanical properties.[12] For example, when the droplets

55 are used as a template to fabricate micro/nano particles for the drug delivery system, the shape

56 and size of emulsion droplets have significant impacts on the drug release kinetics.[13-

57 [14]Monodisperse droplets with precisely controlled sizes can be used to deliver an accurate dosing

58 of contained payload such as drug, flavoring, or chemical reactants.[15] Therefore, monodispersity

59 and size tenability are highly desired for ensuring that the droplets exhibit constant, controlled

60 and predictable behaviors.[4,12] However, the complex rheological properties of non-Newtonian

61 fluids challenge the versatility in droplet size control. For example, the stretching and/or thinning

62 of non-Newtonian liquid filaments will lead to the formation of "bead-on-string" patterns.[16-

63 [17]These beads can subsequently become undesirable satellite droplets, increasing the

64 polydispersity of the resultant droplet population.The dynamics of the droplet formation process

65 can be characterized into a dripping and a jetting regime. The dripping-to-jetting transition can

66 be estimated using the Capillary number of the continuous phase, Ca_{out}, a ratio of viscous force to

67 surface tension, and the Weber number of the dispersed phase, We_{in}, a ratio of inertial force to

68 surface tension.[18]

69
$$We_{in} = \frac{\rho_{DP} d v_{DP}^2}{\sigma} \tag{1}$$

70
$$Ca_{out} = \frac{\eta_{CP,0} v_{CP}}{\sigma} \tag{2}$$

71 where ρ_{DP} is the density of dispersed phase, d refers to the diameter of the orifice, V_{DP} and V_{CP}

72 are the velocities of dispersed and continuous phase respectively, σ is the interfacial tension,

73 and $\eta_{CP,0}$ is the apparent viscosity of the non-Newtonian fluid of continuous phase. The subscript

74 "0" refers to zero-shear rate when a shear-dependent fluid is used. Droplet formation occurs at

75 the orifice directly after the two fluids meetin the dripping process, when both Ca_{out} and We_{in} are

76 small, as surface tension dominates. By contrast, jetting occurs when Ca_{out} or We_{in} is large, as the

77 viscous stress or the inertial force on the droplet will be large enough to overcome surface

78 tension. Droplets are generated after breakup of a jet at some distance downstream in this

79 regime.While the dynamics of droplet breakup has been systematically investigated in

80 Newtonian fluids,[17-18] the validity of the understanding has not been adequately confirmed in

81 non-Newtonian fluid systems. In addition, a number of non-Newtonianfluids such as polymeric

82 solutions, whole blood orprotein solutions with large polymeric molecules often exhibit elastic

83 property due to the stretching and coiling of the polymer chains. The resultant non-Newtonian

84 rheological behaviors inspire interesting applications.[19]For instance, microparticles driven in

85 viscoelastic solutions can migrate toward the centerline of a microchannel because of the first

86 normal stress difference between the centerline and the walls; three-dimensional (3D) particle

87 focusing can be achieved via a synergistic combination of inertial andelastic forces. [20]The

88 elasticity of the focusing fluid has been shown to facilitate formation of smaller droplets.[21]These

4

89   examples attests to the need for a comprehensive understanding of the role of elastic fluids with

90   shear-rate-dependent viscosity in droplet formation using microfluidic systems.

91   In this paper, we focus on a shear-thinning fluid, which is one of the most frequently

92   encountered non-Newtonian fluids,[22] and investigate the dripping-to-jetting transition of a

93   Newtonian/shear-thinning two-phase system and characterize the formation of satellite drops in

94   the model system. The breakup time and droplet size are compared with Newtonian/Newtonian

95   two-phase system at the same Weber number and Capillary number.We demonstrate that the

96   degree of control over droplet size can be enhanced by adjusting the flow rate and nozzle size,

97   thus tuning the shear rate experienced by the non-Newtonian fluids. We also present an

98   experimental study of the elasticity effect of a shear-thinning fluid on droplet generation in a

99   microfluidic two-phase system. The shape of the droplets are shown to vary with the

100   Weissenberg number, which represents a ratio of the relaxation time to the hydrodynamic time.

101   Our work helps to elucidate the effects of rheological behaviors on the breakup dynamics in a

102   Newtonian/non-Newtonian two-phase microscaled flow; our understanding inspires new

103   approaches to control sizes and shapes of functional droplets in applications requiring the use of

104   non-Newtonian fluids.

2. Numerical model

106   The microcapillary co-flow device has been widely used in emulsion generation.[23]A3D

107   numerical model with the same design is established in the present investigation (see Fig.1a). A

108   Newtonian fluid is injected in a cylindrical capillary as the dispersed phase at a constant mean

109   velocity V_{DP}. This inner fluid is surrounded by a non-Newtonian outer phase, which is injected

110   through the coaxial square capillary as the continuous phase at a constant mean velocity V_{CP}. The

111   cross section (perpendicular to the main flow direction) consists of a circle inside a square (see

112   inset of Fig.1a). Thus, the continuous phase is flowing through a cross section between an inner

113   circle and outer square. No-slip condition is applied at the solid boundaries of the walls of

114   capillaries. Gauge pressure of zero is applied at the outlet of the domain. The maximum entrance

115   length is 9.4 μm in our numerical computations, and the length of the computational domain is 6

116   mm, which is long enough to ensure that the fluid flow can be fully developed. The governing

117   equations for incompressible two-phase fluids are,[24]

$$\frac{\partial \alpha_{CP}}{\partial t} + v \cdot \nabla \alpha_{CP} = 0 \tag{3}$$

$$\frac{\partial \rho}{\partial t} + \nabla \cdot (\rho v) = 0 \tag{4}$$

$$\frac{\partial}{\partial t}(\rho v) + \nabla \cdot (\rho v v) = -\nabla P + \nabla \cdot [\eta(\nabla v + \nabla v^T)] + \frac{\rho \sigma \nabla \alpha_{CP}}{\frac{1}{2}(\rho_{DP} + \rho_{CP})} \nabla \cdot \frac{\nabla \alpha_{CP}}{|\nabla \alpha_{CP}|} \tag{5}$$

$$\rho = \alpha_{CP}\rho_{CP} + (1 - \alpha_{CP})\rho_{DP} \tag{6}$$

$$\eta = \alpha_{CP}\eta_{CP} + (1 - \alpha_{CP})\eta_{DP} \tag{7}$$

123   where v is the flow velocity, P is the pressure, ρ is the volume averaged density, α_{CP} and ρ_{CP} are

124   the volume fraction and density of the continuous phase respectively, η_{DP} and η_{CP} are dynamic

125   viscosities of the dispersed and continuous phases, respectively. The 3D numerical volume of

126   fluid (VOF) model has been implemented to investigate the droplet breakup in pair of non-

127   Newtonian/Newtonian fluids in T-shaped microchannel.[24]The rheological property of the non-

128   Newtonian continuous phase is modeled using Cross model, which has been widely applied in

129   the modeling of industrial shear-thinning fluids.[25]A shear-thinning fluid is used in our present

130   study and its apparent viscosity is defined by,

131
$$\eta_{CP} = \eta_\infty + \frac{\eta_0 - \eta_\infty}{1 + (\lambda_c \dot{\gamma})^n}$$
(8)

132   where η_∞ refers to lower limiting values of the fluid viscosity or infinite shear viscosity; η_0 refers

133   to upper limiting values of the fluid viscosity or zero shear viscosity; λ_c is the time constant, the

134   reciprocal of which corresponds to a critical shear rate that provides a useful indicator of the

135   onset shear rate for shear thinning; $\dot{\gamma}$ is the shear rate and n represents the power law index of

136   fluid. The solutions with different values of these parameters will have different rheological

137   behaviors. Any effect due to gravity is neglected for simplicity, because the length scale of

138   interest is much smaller than the capillary lengthof 1.33 mm in our model. The two-phase flow is

139   solved using the VOF method by CFD software Ansys Fluent 14.0. The approach has been

140   successfully demonstrated to investigate multiphase flow in microsystem.[26]The governing

141   equations are discretized to algebraic equations by using a control-volume-based technique. An

142   iterative solver was deployed to solve the control-volume discretized equations. The iterative

143   timestep is 10^{-7} s and the solution converges when the residual is below a tolerance set as 1.0

144   x10^{-6}.The simulations were performed using numerical grids composed of triangular elements, as

145   shown in Fig.1b.The numerical data was subsequently analyzed by Ansys CFX-Post 14.0 after

146   simulation was completed. Computational sensitivity study has been carried out to evaluate the

147   effect of different triangular grid sizes. The generated morphology of interface as indicated by

148   the green color between dispersed and continuous phases is compared using different grid sizes.

149   Similar morphology is found at flow rates of the dispersed phase Q_{DP}=50 ml/h, and of the

150   continuous phase Q_{CP}=70 ml/h, as shown in Fig.2. The size of interface gradually increases

151   along the axial direction, and subsequently adopts cylindrical shape downstream with a uniform

152   size for grid sizes of 4 μm and 8 μm.The variation in the generated size of interface is less than 5%

153   after convergence between grid sizes of 4 μm and 8μm. Furthermore, we investigated the grid

154   size effect by comparing numerical results of axial velocity profile along transversal direction (x

155   direction) for different grid sizes, at two downstream locations, z=0.02 mm, where the two

156   phases meet in vicinity of orifice, and z=5.27 mm, where the flow has become fully developed,

157   as shown in Fig.3a-b, respectively. At z=0.02 mm, the sharp peak in the middle represents the

158   velocity profile of dispersed phase, which is purged out of orifice with very small size, thus the

159   velocity will be increased dramatically due to mass conservation. The magnitude of velocity for

160   the continuous phase is much smaller, because of the much larger cross section.At z=5.27 mm,

161   the velocity profiles of dispersed and continuous phases adjoin with a smooth transition at the

162   interface. Compared with coarse grids with a size of 12 μm, a good agreement is found between

163   refined grids with a size of 4 μm and 8 μm respectively. 4300956 triangular elements with a size

164   of 8 μm are used in all the following numerical simulations to reduce computation cost.

165

166
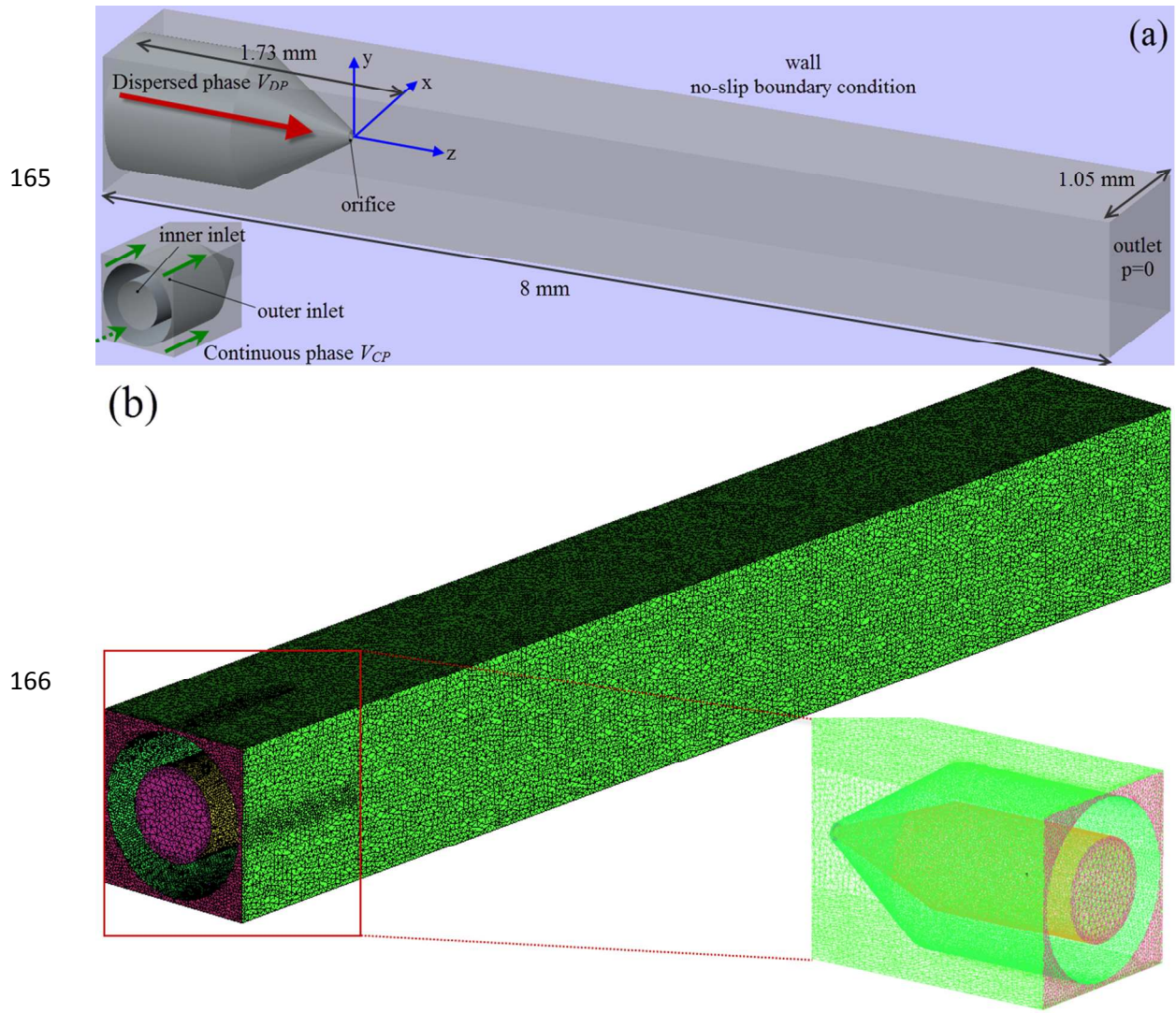
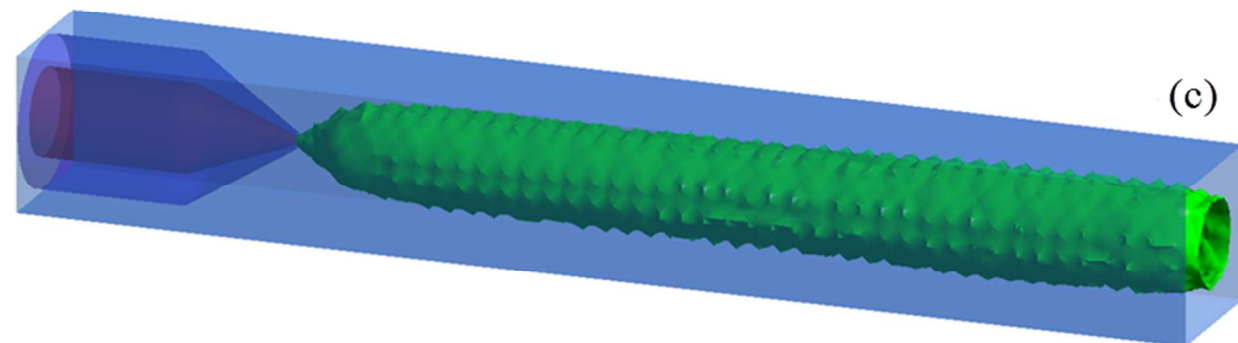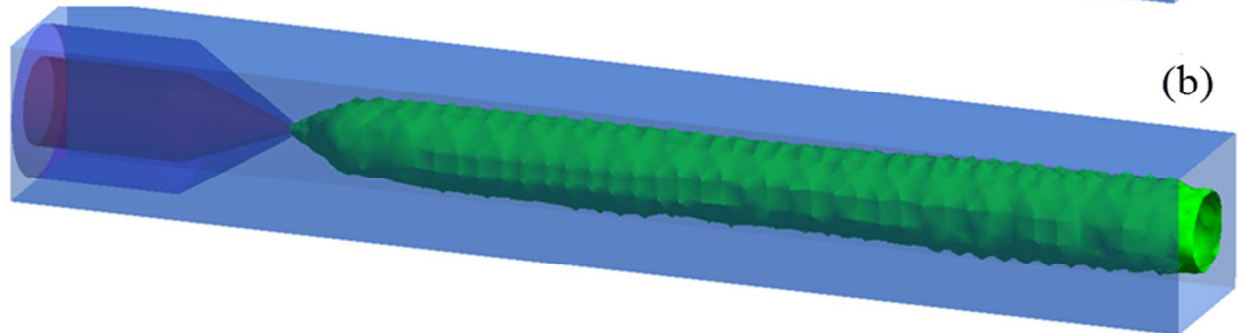167   **Fig.1**(a) Schematic of the computational domain of multiphase microfluidic system. (b) Meshing

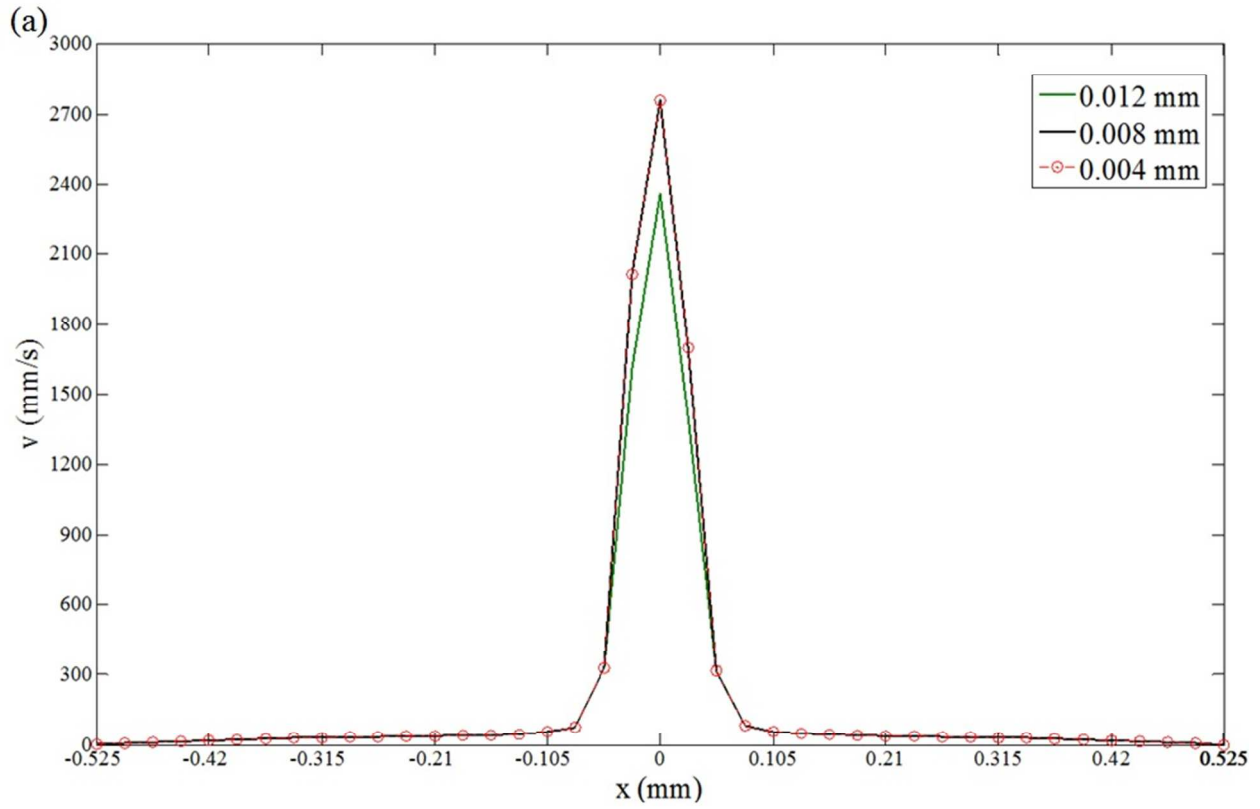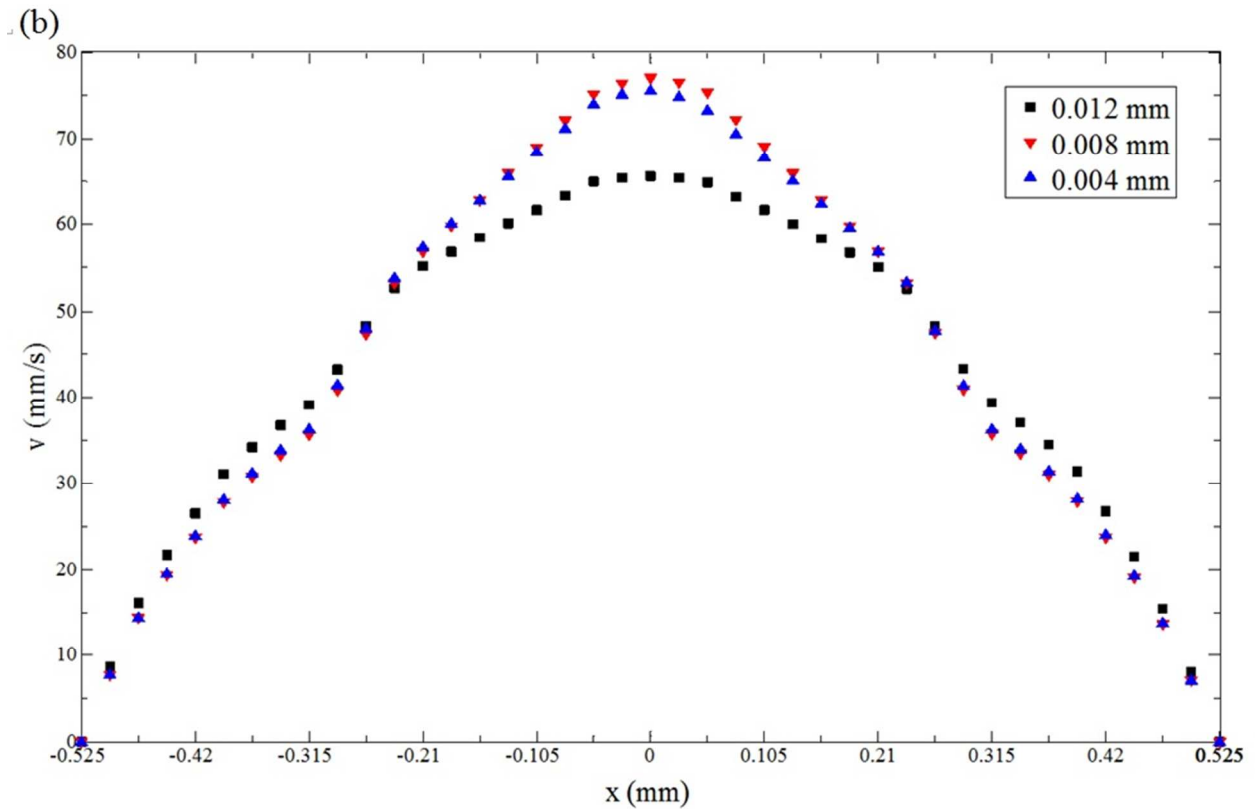168   grids.The close-up view of meshing of nozzle and inlets is shown in inset.

169

170
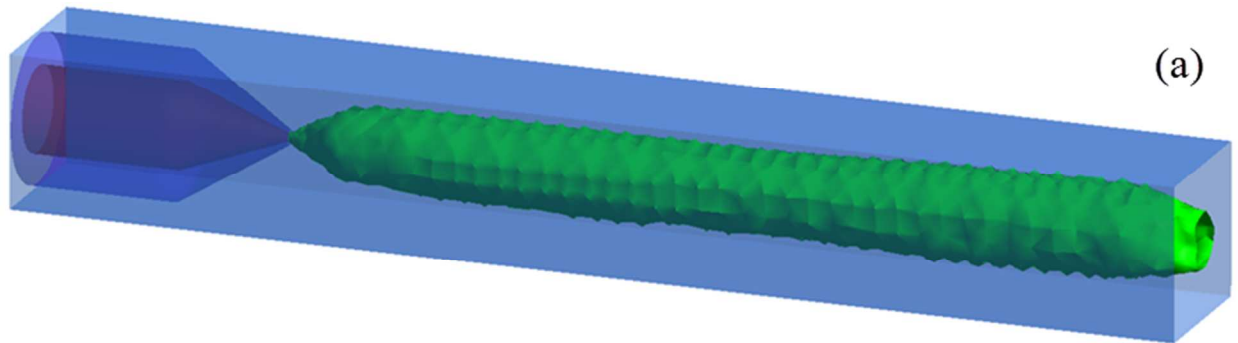
171

172   **Fig.2** Comparison of morphology of jet using different meshing grid sizes (a) 0.012 mm (b)

173   0.008 mm and (c) 0.004mm. Q_{DP}=50 ml/h, Q_{CP}=70 ml/h.

174

175

176 **Fig.3** Validation of the numerical model of Newtonian/shear-thinning multiphase microfluidic

177 system by comparison of axial velocity profile along transversal direction (*x* direction) at (a)

178 *z*=0.02 mm and (b) z=5.27 mm using different meshing grid sizes.

3. Experimental section

179

180 The Newtonian/shear-thinning two-phase co-flow is generated using a glass microcapillary

181 device reported earlier.[23]A glass slide was used as a substrate to support the capillary device,

182 which is composed of an inner round capillary (World Precision Instruments, Inc) and an outer

183 square capillary (Atlantic International Technology, Inc.).The round capillary has inner and outer

184 diameters of 630 μm and 1.0 mm, and its tip was tapered to the desired diameter by a

185 micropipette puller (Sutter Instrument, Inc.) to obtain an orifice with an inner diameter of about

186 49 μm. The tapered round capillary was fitted into the square capillary, which has an inner

187 dimension of 1.05 mm.Sincethe outer diameter of the round capillary matches with the inner

188 dimension of the square capillary, coaxial alignment of the two capillaries is ensured. The

189 dispersed phase was injected into the device through the circular capillary, while the continuous

190 phase was injected in the same direction through the square capillary. The fluids were injected

191 into the device through a flexible plastic tubing (Scientific Commodities Inc.), which was

192 connected to syringe pumps (Longerpump, LSP01-2A) at controlled flow rates. Unless otherwise

193 specified, the chemicals used in the study were supplied by Aladdin Reagents (Shanghai) Co.,

194 Ltd. In the present study, the dispersed phase was silicon oil, while the continuous phase was 2%

195 (w/v) aqueous solution of sodium carboxymethyl cellulose (CMC) (Mw=250,000 Da, DS=1.2),

196 which is a pseudo-plastic fluid and demonstrates shear-thinning behaviors. The rheological

197 behavior of CMC solution can be characterized by two critical concentrations: [27]a first critical

12

198 CMC concentration indicates the transition to the semidilute network solution, while a second

199 critical CMC concentration indicates the transition to the concentrated solution. Below the

200 second critical concentration, the CMC solution becomes highly viscous and the dynamics is

201 dominated by viscous effects; above the second critical concentration, the dynamics become

202 dominated by elastic effects. For CMC solution with a nominal molecular weight of 700,000 Da

203 and a degree of substitution of 0.65-0.85, the first critical concentration is ~1% while its second

204 critical concentration is 2.5%.[27]The effect of concentration and molecular weight on the

205 rheological behavior of aqueous CMC solutions has been investigated experimentally.[28]Based on

206 their measurements of the rheological properties, solutions of CMC with molecular weights of

207 90,000 Da, 250,000 Da, and 700,000 Da all exhibit predominantly shear-thinning behaviors over

208 a shear rate of 0-1000 /s in absence of yield stress as their concentration changes from 0.1% to

209 3.0%. The average shear rate of CMC solution is below 1000 /s by controlling flow rate in our

210 work. Therefore, it is reasonable to assume that our CMC solution (Mw=250,000 Da, DS=1.2)

211 still has a predominantly viscous behavior; and the elastic effect can be ignored.[28]

212 We also prepared 5% (w/v) aqueous solution of polyacrylamide (PAA, supplied by Wing Hing

213 Chemical Co., Ltd) as the continuous phase to investigate the elastic effect on the breakup

214 dynamics and droplet formation. The flow behavior inside the microcapillary device was

215 monitored with an inverted microscope (Motic, ocular: WF10×18mm, object lens: EA4). A high-

216 speed camera (Phantomv9.1 high speed camera) was connected to the microscope and the flow

217 through the capillary was captured. The dripping-to-jetting transition using non-Newtonian

218 systems was characterized experimentally, and the breakup dynamics in a non-Newtonian fluid

219 system was compared with a Newtonian fluid system at the same Weber number and Capillary

220 number using the same microdevice. For the Newtonian two-phase flow, silicone oil was also

221   used as the dispersed phase, while 17% w/v aqueous solution of polyethylene glycol (PEG)

222   (Mw=8,000 Da) was used as the continuous phase. The interfacial tension was measured by a

223   Krussspinning drop tensiometer-SITE100. The respective viscosity of each solution was

224   measured at different shear rates by a Brookfield DV-II+Pro programmable viscometer. Shear-

225   thinning behavior of the CMC solution was observed experimentally. The rheology data of CMC

226   solution at all concentrations can be well represented by the well-known Cross model;[27]therefore

227   Cross model was used in curve-fitting of the experimental data, and the measured Cross model

228   parameters (the zero shear viscosity η_0=253.5 cP, infinite shear viscosityη_∞=60 cP, and the

229   flow index n=0.9, as shown in Fig.4) were used in the simulation for computing the simulation

230   results, which were subsequently compared with the experimental observations. Very small

231   variations of viscosity were observed at different shear rates (see Fig.4), indicating that 17% w/v

232   PEG solution exhibits largely Newtonian properties. The concentration of PEG solution can

233   affect the rheological property. For example, 7% w/w PEG solution shows significantly different

234   viscosity values at different shear rates, demonstrating a non-Newtonian behavior.[29]5% w/v PAA

235   solution possesses shear-thinning behavior, as shown in Fig.4. As a typical viscoelastic liquid,

236   the rheology property of PAA has been well investigated, and the storage modulus G' and loss

237   modulus G" have been measured using the oscillatory shear rheometer.[30]Based on the reported

238   data, we find the relaxation time λ=0.017 s, according to Maxwell model of viscoelastic

239   liquid.[31]The relevant dimensionless numbers of viscoelastic liquid include Weissenberg number

240   *Wi* and Elasticity number *El*. The Weissenberg number is defined as the product of the relaxation

241   time and a characteristicrate of deformation of the flow, and quantifies the nonlinear response of

242   the liquid.

243
$$Wi = \frac{\lambda U}{D_t} = \frac{\lambda Q_{CP}}{D_t^3} \qquad (9)$$

14

244   where U is the average axial flow velocity in the capillary device and D_t refers to the dimension

245   of the capillary tube. Wi is dependent on flow rate and varies in the range between 0.0041 and

246   0.041 in our experiments. The ratio between elastic and inertial effects is represented by the

247   Elasticity number,

248    $$El = \frac{Wi}{Re} = \frac{\lambda \eta_{CP,0}}{\rho_{CP} D_t^2} \tag{10}$$

249   where Re refers to Reynolds number. El is thus independent on the flow rate based on the

250   definition. In our experiments El=382, indicating the dominating role of elastic effect relative to

251   inertia effect. The physical properties of the fluids used in the investigation are shown in Table 1.
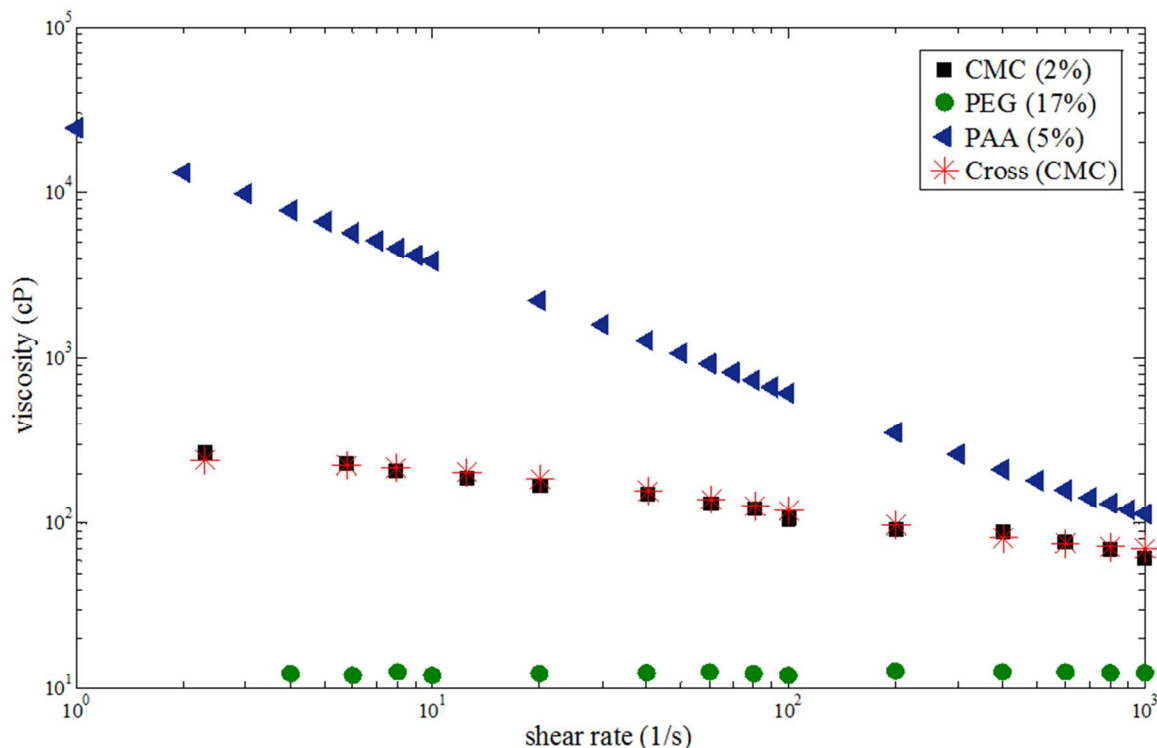
252

253   **Fig.4** Rheological properties of the three aqueous polymer solutions: 2% w/v sodium

254   carboxymethyl cellulose (CMC) in water (black squares), 17% w/v polyethylene glycol (PEG) in

255   water (green circles), 5% w/v polyacrylamide (PAA) in water (blue triangle) and Cross model of

256   CMC solution(red cross).

257
258 **Table 1**

259 Physical property of the test fluids

Test fluids	η (cP)	ρ (g/ml)	σ (mN/m) (silicon oil and CMC)	σ (mN/m) (silicon oil and PEG)	σ (mN/m) (silicon oil and PAA)
Silicon oil	10	0.963			
CMC (2%)	253.5 (zero-shear rate)	0.990			
PEG (17%)	13.6	1.053	7.12	9.624	10.176
PAA (5%)	24569(zero-shear rate)	0.992			

260

261 # 4. Results and discussion

262 The breakup dynamics and dripping-to-jetting transition in Newtonian/shear-thinning multiphase

263 microsystem are presented and discussed first, followed by discussion of elastic effect in droplet

264 shape at the end of this section. Simulation and experiments of Newtonian/shear-thinning

265 multiphase flow in the capillary microdevice have been conducted under the same flow

266 conditions to observe the process of jet deformation and droplet formation. Silicon oil and CMC

267 solution are used as dispersed phase and continuous phase, respectively.The flow pattern at

268 successive time points from simulation is shown in Fig.5. The flow rates of the dispersed and

269 continuous phasesare 5 and 7 ml/h, respectively, with Ca_{out} =0.0631 and We_{in} =5.147. The

270 transition regime is observed and the jet size changes along the length of jet. The dispersed phase

271 is purged out of the orifice, as shown by the inset in Fig.5a.The droplet grows in size and moves

272 downstream while it is still connected to the fluid neck through the orifice via a filament, as

273 shown in Fig.5b. The filament gradually becomes thinner (see Fig.5c) and finally breaks up intoa

274 droplet (see Fig.5d). The process is repeated afterwards. The interface between the two phases in

275 Fig.5d is tracked by plotting the radius of interface along transversal direction (y direction)

276 versus the streamwise location along z direction. The simulation result is represented by the solid

277 line, and is compared with experimental measurements indicated by the symbols. A reasonable

278 agreement, as shown in Fig.5e, validates the accuracy of the numerical model.

279 A satellite droplet is formed during the breakup of an elongated filament between two adjacent

280 droplets. The profile near the breakup point is highly asymmetric, with the droplet interface

281 being very steep towards the droplet while lying flat towards the neck of the jet. The existence of

282 satellite drops is intimately related to the non-linear properties of the fluid motion close to the

283 breakup point.[32]When the filament breaks at both ends before merging with one of the parent

284 droplets, the filament separates from both neighboring parent droplets and recoils into a satellite

285 droplet.[33]The number of satellite droplets and their relative sizes strongly depend on the viscosity

286 ratio of the dispersed phase to that of the continuous phase, and are also influenced by the initial

287 disturbance wavenumber, which is defined as $2\pi a/\varepsilon$, where a is the radius of filament and ε is the

288 wavelength.[34]At a small viscosity ratio, the slender center droplet undulates and pinches off at a

289 number of locations, generating a string of small satellite droplets. By contrast, when the

290 viscosity ratio is large, the internal flow leading to breakup is attenuated, resulting in the

291 formation of fewer satellite droplets. As the wave number increases, the ratio of radius of

292 satellite droplets in different birth regions relative to radius of parent droplet also increases.[34]

293

294
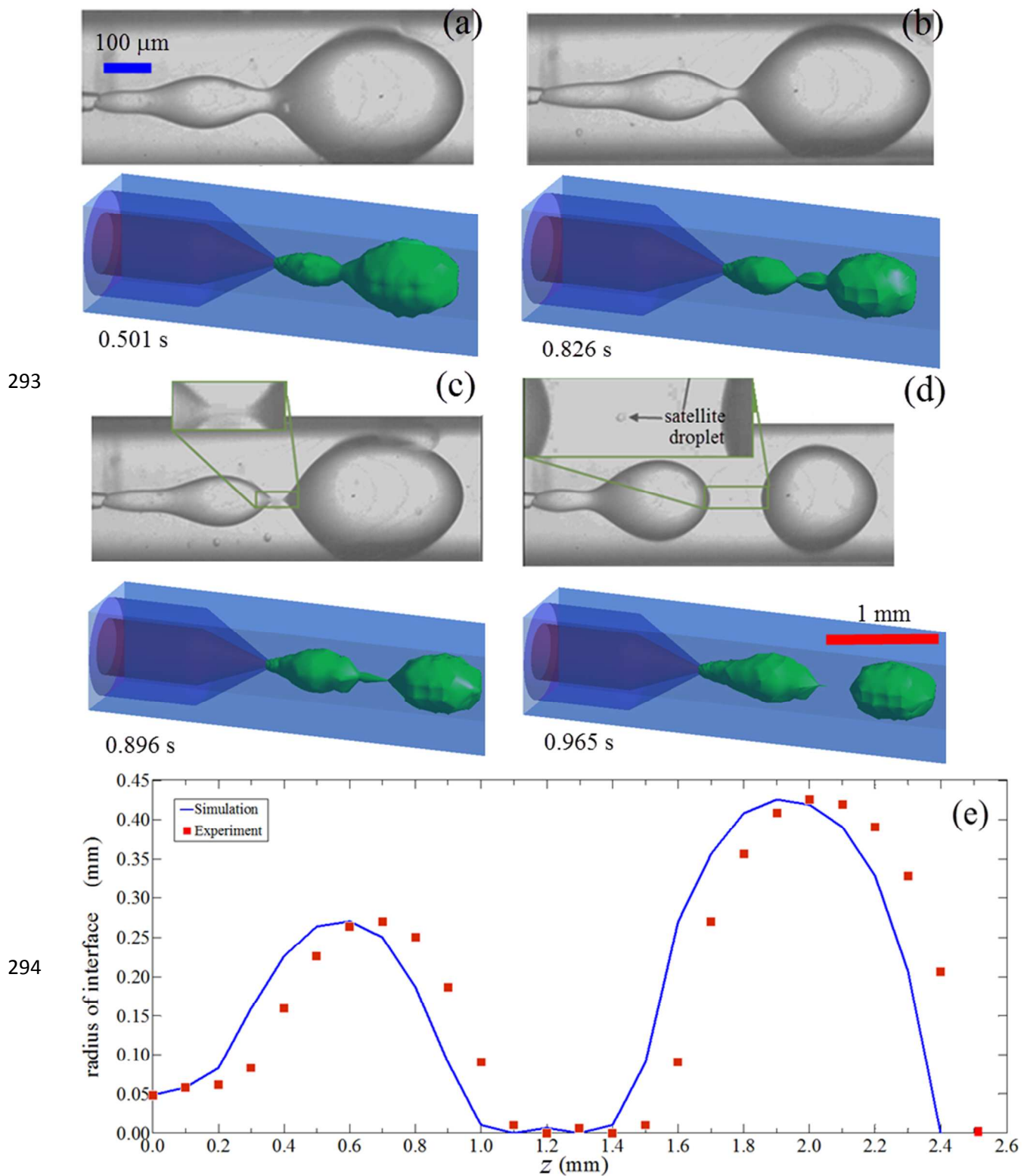
295 **Fig.5** Time-lapse images of jet deformation and droplet formation from simulation (upper one in

296 each sub-figure) and experiments (lower one in each sub-figure) using a Newtonian/shear-

18

297   thinning two-phase co-flow system (silicon oil as dispersed phase and CMC solution as

298   continuous phase). The blue and red scale bars are applicable for the experimental and

299   simulation results respectively. (a) The dispersed phase is purged out of the orifice; (b) The main

300   droplet is connected with the fluid neck via a thin filament; (c) The filament becomes even much

301   thinner; (d) Satellite dropletoccurs after breakup of the jet; (e) Tracking of interface profile by

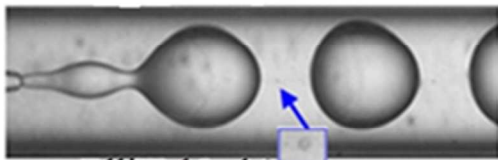302   both simulation and experimental observation.

303   Since the satellite droplets have a much smaller size than the main droplet, the global

304   polydispersity of the resultant emulsion increases. To predict the occurrence of satellite droplets,

305   the flow conditions that result in the formation ofsatellite droplets have been delineated using a

306   state diagram, which shows the two-phase flow pattern as a function of Weber number and

307   Capillary number.Three representative flow regimes are observed when the flow rate ratio is

308   varied, as shown in Fig.6a: dripping, where droplets are formed in the vicinity of the capillary tip;

309   intermediate, where the growing droplets move downstream while remaining connected to the

310   fluid in the tip through a fluid neck;[18]and jetting, where droplets breaks up from an extended jet

311   with an incomplete retraction of the fluid neck. For the intermediate regime, the fluid neck

312   retracts completely back to the tip after the droplet pinches off at the detachment point of the

313   fluid neck. This regime is thus still regarded as dripping.[18]Upon further increase of viscous or

314   inertia force, for instance, by changing the flow rate of continuous or dispersed phase, the

315   intermediate regime will transition to the jetting regime. Comparison of results from simulation

316   and experiments shows a good agreement, confirming the validity of our model in capturing the

317   physical behavior of the two-phase flow when a non-Newtonian fluid is used. As We_{in}

318   increases,the viscosity of the shear-thinning continuous phase decreases, when subjected to high

319   shear rate. As a result, a lower viscousstress is exerted on the dispersed phase; the liquid thread is

320 therefore not pulled further downstream. Consequently, the flow remains in the intermediate

321 regime rather than in the jetting regime. However, when We_{in} is larger than 10, jetting occurs

322 because of the larger inertial force. Based on experimental observation, satellite droplets appear

323 only in the intermediate regime, which is characterized as a dripping-to-jetting transition,[18] as

324 shown in the state diagram in Fig.6b. Inertia is necessary to induce the formation of a satellite

325 droplet, because the droplet formation will be suppressed when the viscous force is dominant

326 over inertia. However, a very large inertial force will lead to formation of jetting and the liquid

327 thread will breakup into droplets further downstream. Consequently, the pinch-off time increases,

328 delaying the formation of the parent droplet and satellite droplets. This state diagram can help

329 predict the formation of undesirable satellite droplets in a Newtonian/shear-thinning two-phase

330 system, and can suggest operating conditions for eliminating satellite droplets. This ultimately

331 inspires production of monodisperse droplets by manipulating the breakup profile and

332 controlling the merging of satellite droplets with main droplets; yet these investigations are

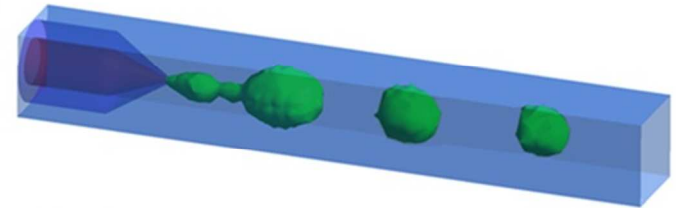333 beyond the scope of the present study.
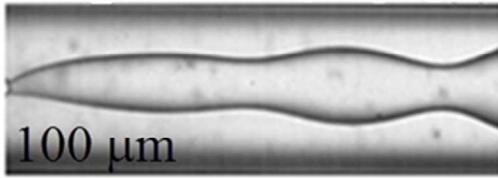
(a) Dripping (Ca_{out}=0.045, We_{in}=0.052)
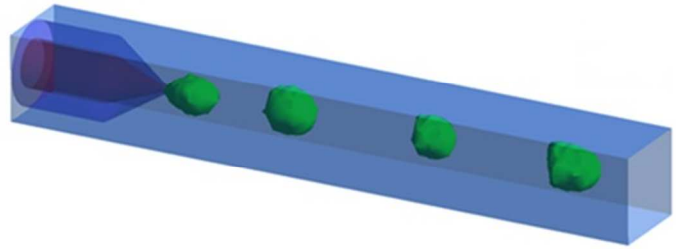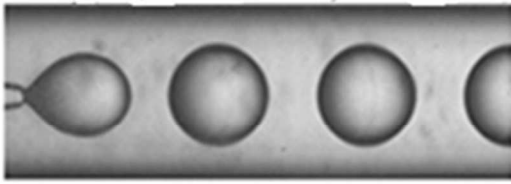
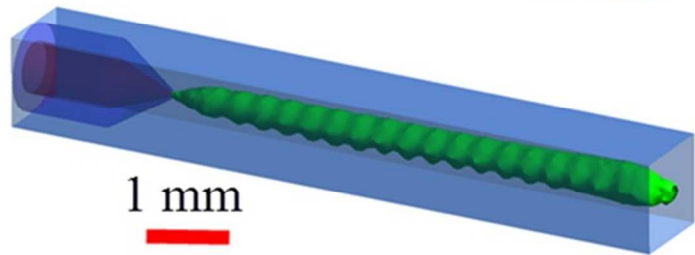Intermediate (Ca_{out}=0.091, We_{in}=5.15)

satellite droplet
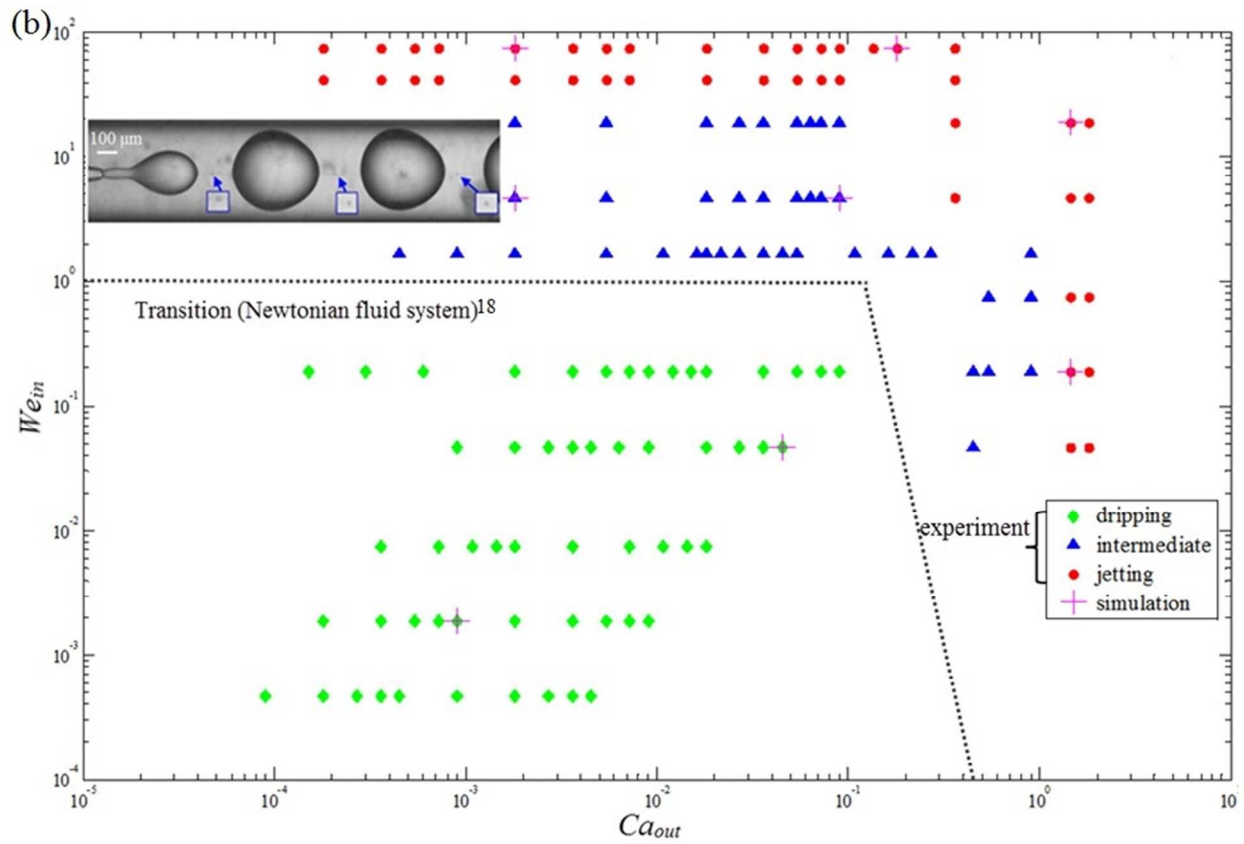
Jetting (Ca_{out}=0.18, We_{in}=82.29)

100 μm

1 mm

(b)

100 μm

Transition (Newtonian fluid system)[18]

experiment

- dripping
- intermediate
- jetting
+ simulation

We_{in}

Ca_{out}

334

335

336   **Fig.6**(a) Comparison of results from simulation and experiments at different regimes using a

337   Newtonain/shear-thinning two-phase coflow system (silicon oil as dispersed phase and CMC

338   solution as continuous phase).The blue and red scale bars are applicable for the experimental and

339   simulation results respectively. (b) State diagram showing the dripping-jetting transition as a

340   function of Ca_{out} and We_{in}.The inset shows the satellite droplets appearing periodically between

341   adjacent parent droplets. The dash line (reproduced from reference.[18]) shows the dripping-to-

342   jetting transition in a purely Newtonian two-phase coflowsystem (deionized water and

343   polydimethylsiloxane (PDMS) oils).

344   The breakup time is one of the determining factors on the droplet production rate. It is thus of

345   fundamental interest and industrial relevance to investigate the breakup time when non-

346   Newtonian fluids, for example, shear-thinning fluids, are used, in comparison to the counterpart

347   of Newtonian multiphase system at the same We_{in} and Ca_{out}. Droplet breakup occurs due to the

348   interplay between the viscous stress and the interfacial tension between the two fluids. The

349   viscous stress is closely associated with the shear rate, which varies greatly depending on the

350   position and the shear rate, which affects the viscosity in all directions in the 3D flow. The

351   highly deformed filament connecting the fluid neck with the droplet (see Fig.5b) is of particular

352   interest, because it is the region where breakup occurs. We will therefore use the filament region,

353   for instance, z=0.87 mm, as the focal point to characterize the shear-rate-dependent viscosity

354   profile. Given the continuity of velocity at the interface and the small diameter of filament, the

355   shear rate reaches a sharp peak at the interface between the two phases in the filament region.

356   Due to shear-thinning characteristics of CMC solution, the viscosity will be dramatically reduced

357   at the interface, as shown by the numerically calculated results of viscosity and shear rate as a

358   function of the radial location along the transverse direction of the capillary device in Fig.7. The

359   shear rate of the continuous phase in the co-flowing microfluidic device with a dimension of D_t is

360   related to the droplet diameter D_d through,[26]

361
$$\dot{\gamma} \sim \frac{Q_{CP}}{\pi D_t{}^3 \left[1 - \left(\frac{D_d}{D_t}\right)^2\right]\left(1 - \frac{D_d}{D_t}\right)} \tag{11}$$

362   Given the flow condition in Fig.5, where Q_{CP}=7 mL/h and $\frac{D_d}{D_t} = 0.5$, $\dot{\gamma} \sim 1.65/\text{s}$. The calculated

363   shear rate of the continuous phase is of the same order of magnitude as the simulation result. A

364   local maximum shear rate of 9.68/s for continuous phase is obtained at the wall of collection tube,

365   because of no-slip at the wall and large velocity gradient in boundary layer adjacent to the wall.

366   The shear rate is reduced in the region far from the wall, and the minimum value of 3.87/s is

367   obtained at r=0.375 mm.

368
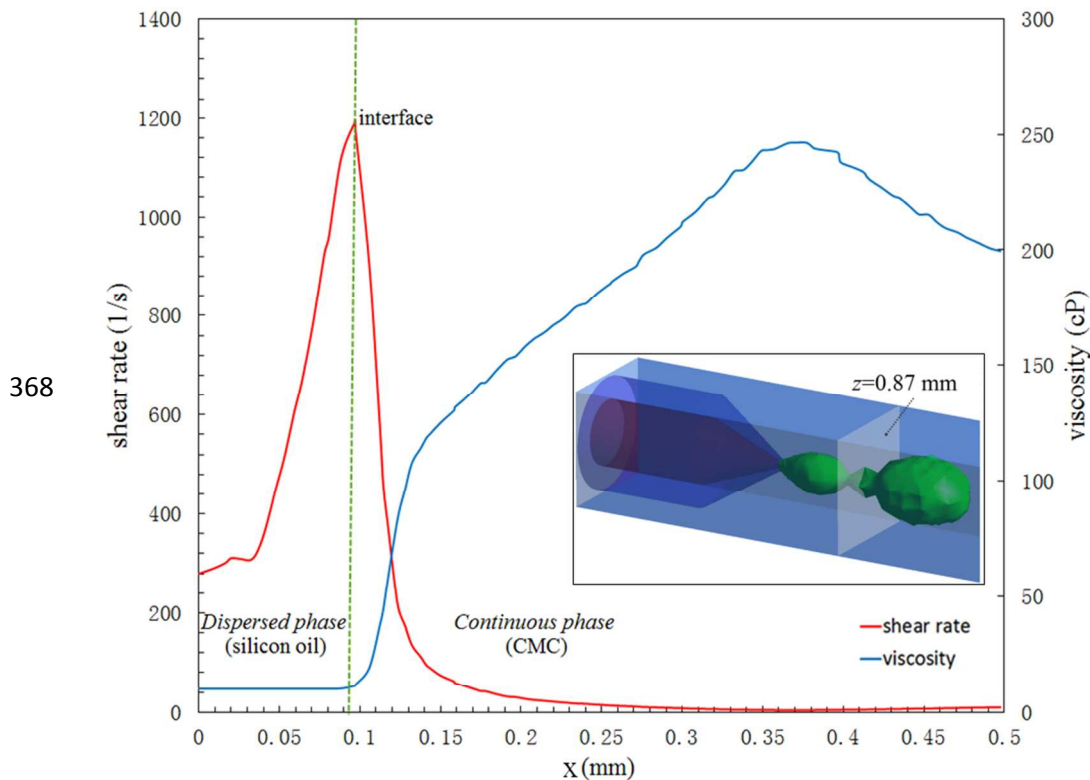
369   **Fig. 7** The numerically calculated viscosity and shear rate as a function of the radial position

370   along the transverse direction of the capillary device of the Newtonian/shear-thinning two-phase

371   coflow system (silicon oil as dispersed phase and CMC solution as continuous phase) at z=0.87

372   mm, which is illustrated in inset.

373   For shear thinning fluids, the viscosity is inversely proportional to the shear rate; thus the viscous

374   effect will be attenuated near regions with high shear rate, facilitating the pinchoff of the jet.

375   Consequently, the breakup process will be sped up so that a higher production rate of droplets

376   can be expected. To verify the hypothesis that shorter breakup time can be achieved when a

377   shear thinning fluid is involved, control tests have been conducted to monitor the breakup time

378   for the purely Newtonian two-phase system. The dimensionless pinching time,

379    $\hat{t}_p = t_p / t_\upsilon = t_p / (\eta_0 d / \sigma)$, was measured experimentally at the same We_{in} and Ca_{out}, where t_p and

380   t_v refer to the measured time interval between two successive pinching, and the viscous time

381   scale, respectively. When compared with the Newtonian system with constant viscosity, the

382   shear-thinning fluid near the liquid-liquid interface has a much reduced viscosity due to high

383   shear rate; as a result, at the same Capillary number, surface force dominates and the pinching is

384   faster when a shear-thinning fluid is used as the continuous phase. The dimensionless breakup

385   time is also reduced when Ca_{out} increases due to the enhanced viscous shear stress exerted on the

386   droplets, as shown in Fig. 8 where We_{in}=1.852.

387
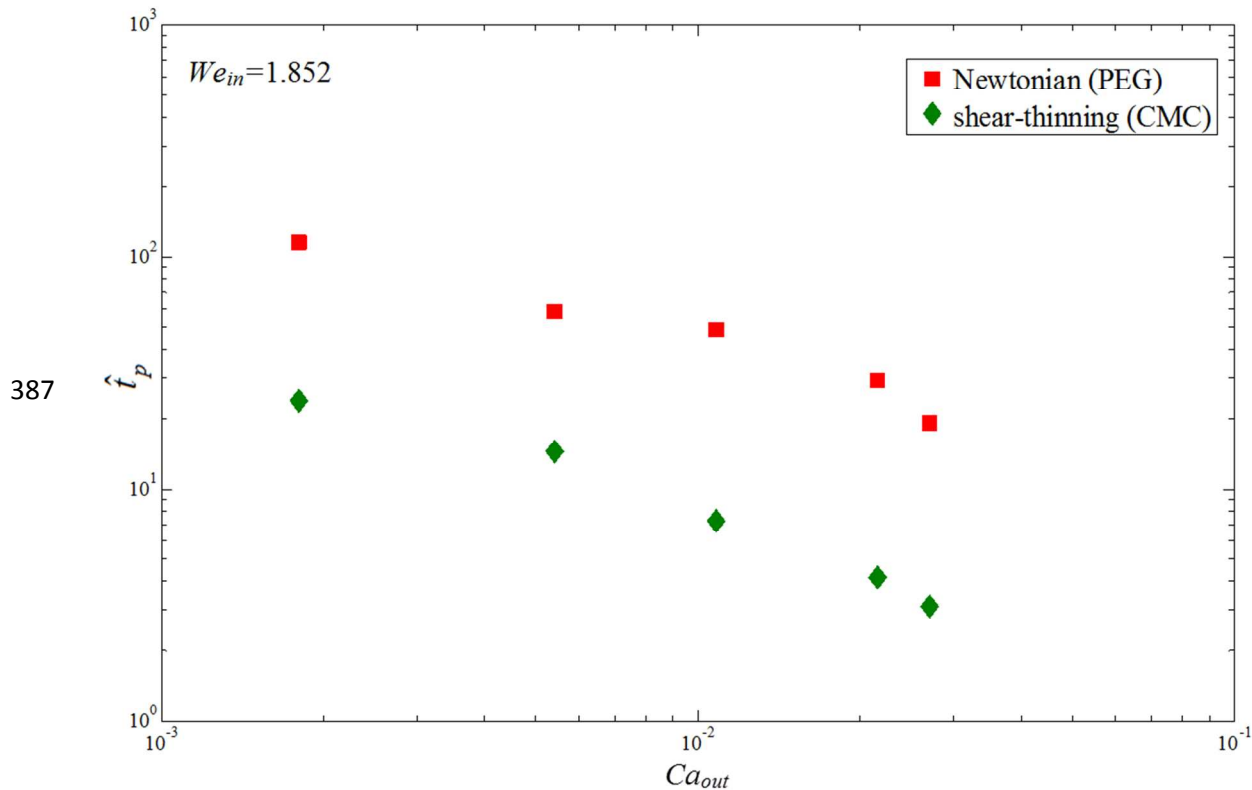
Fig.8 Comparison of the experimentally observed breakup time of jet into droplets using the Newtonian/shear-thinning two-phase coflow system (silicon oil as dispersed phase and CMC solution as continuous phase) versus Newtonian/Newtonian two-phase coflowsystem (silicon oil as dispersed phase and PEG solution as continuous phase) when We_{in}=1.852.

388

389

390

391

In the breakup process of liquid jet of dispersed phase, the droplets are formed and surrounded by the continuous phase. The droplet size is influenced by the viscous force and the surface tension force. Due to the reduced viscosity of the continuous phase, the droplet size is larger when a shear-thinning fluid is used at the same We_{in} and Ca_{out}.[35]This is confirmed by the observed snapshots of droplets after breakup at the same Weber number but at different Capillary numbers in two different multiphase systems, as shown in Fig.9. In both cases, silicone oil is used as the dispersed phase, while solutions of PEG and CMC are used as the Newtonian and

392

393

394

395

396

397

398

399 non-Newtonian continuous phases respectively. At the same Weber number of 1.852, both

400 systems show a decrease in the droplet size when the Capillary number is increased from 0.0018

401 to 0.054 (see Fig.10), due to the higher shear stress and the enhanced hydrodynamic focusing

402 effect by the continuous phase.

403
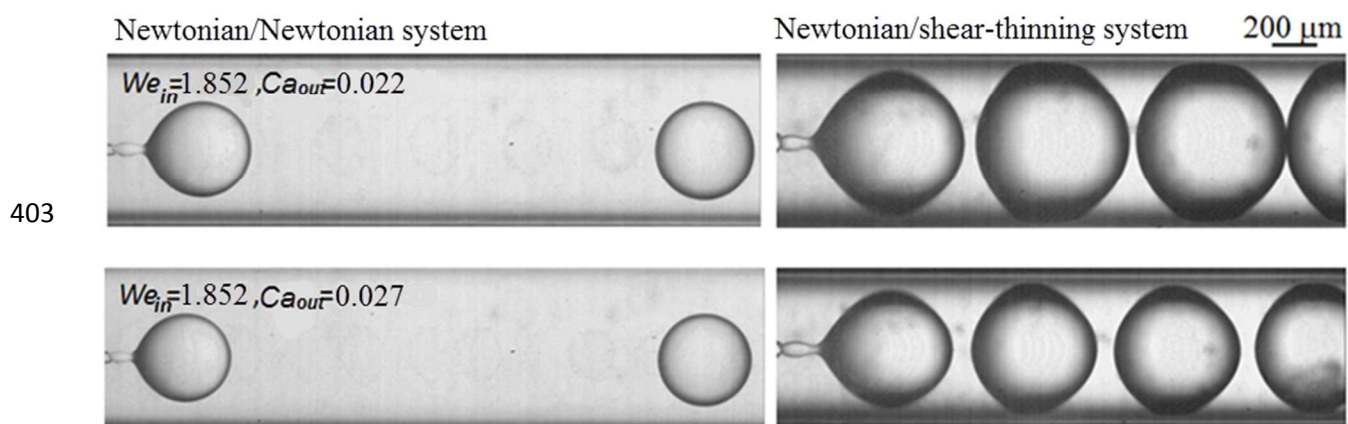
404 **Fig.9** Comparison of droplet size betweenNewtonian/shear-thinning two-phase coflow system

405 (silicon oil as dispersed phase and CMC solution as continuous phase) and

406 Newtonian/Newtonian multiphase coflowsystem (silicon oil as dispersed phase and PEG solution

407 as continuous phase).

408
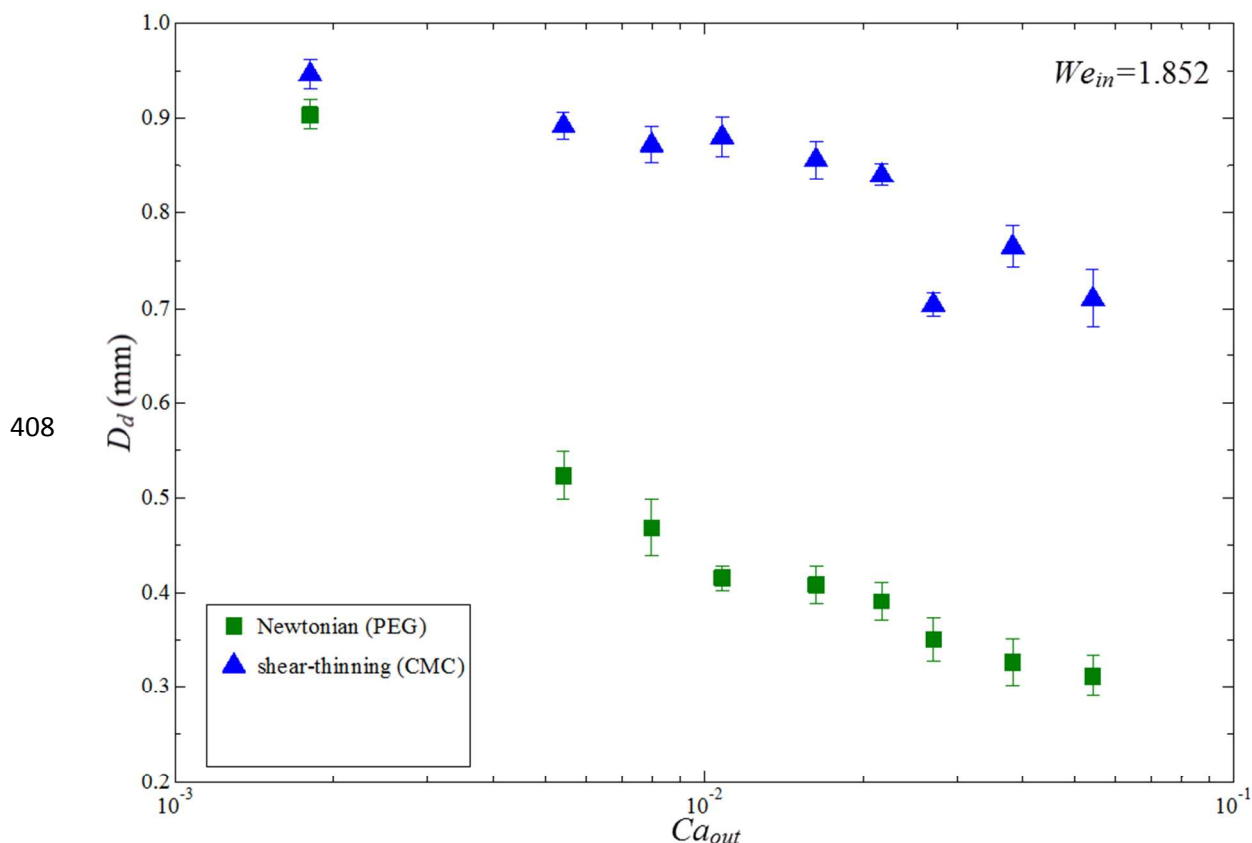
409   **Fig.10**   Comparison   of   the   experimentally   observed   droplet   diameter   between   the

410   Newtonian/shear-thinning two-phase system (silicon oil as dispersed phase and CMC solution as

411   continuous phase) and the Newtonian/Newtonian two-phase system (silicon oil as dispersed

412   phase and PEG solution as continuous phase).We_{in}=1.852 in all cases.

413   Control of the droplet size is also an important aspect of droplet-based microfluidic applications.

414   For example, the volume of the droplet which contains reagents or analytes is one of the key

415   parameters that determinethe efficiency and the overall throughput of the system.[36]Since non-

416   Newtonian fluids are ubiquitous in biochemical applications of microfluidics, it is also crucial to

417   control droplet size. To achieve smaller droplets, we vary the dimensions of the nozzles by

418   fitting a round capillary with radius R into the square capillary (see Fig.11). At a constant flow

419   rate of outer-phase and constant Capillary number, evaluated based on the apparent viscosity, the

420   shear rate increases with decreasing inner diameter of the collection capillary, leading to an

421   increase in the shear stress and thus reduced droplet sizes, as shown by the observed droplets in

422   the collection tube with two different sizes in Fig.11. The droplet size is significantly reduced

423   when collection tube with a smaller radius of 0.3mmis used (see the sub-figures on the right) as

424   compared to that with a radius of 0.5 mm (see the sub-figures on the left), at the same Weber

425   number and Capillary number.
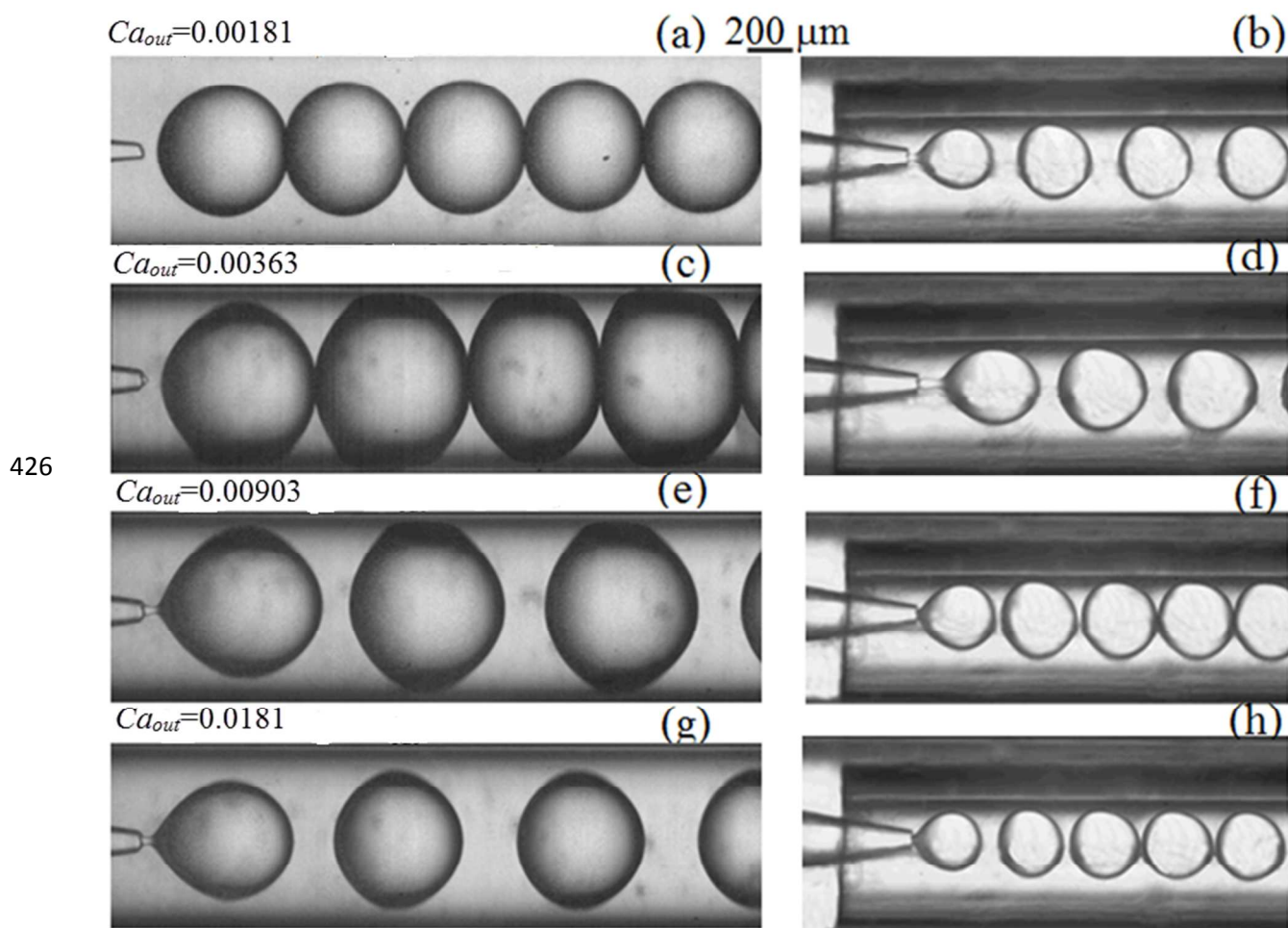
427   **Fig.11** Observed droplets in collection tubes with different sizes ($R=0.5$mmin a, c, e and g;

428     $R=0.3$ mm in b, d, f and h) using Newtonian/shear-thinning two-phase system (silicon oil as

429   dispersed phase and CMC solution as continuous phase).Ca_{out}=0.00181 in a-b, Ca_{out}=0.00363 in

430   c-d, Ca_{out}=0.00903 in e-f, and Ca_{out}=0.0181 in g-h. We_{in}=0.206 in all cases.

431   As Ca_{out} and the shear rate of continuous phase increase, the viscosity of continuous phase is

432   reduced for shear-thinning fluids such as CMC; this results in larger droplets.[35]However, when

433   Ca_{out} increases beyond a critical value, the viscous drag can overcome the surface tension effects

434   that would otherwise minimize the stretching of the fluid neck by drawing the fluid interfaces

435   closer to the orifice. As a result, the fluid neck becomes stretched and elongated at high Ca_{out}.

436   The radius of fluid neck r_j can be characterized by a scaling law that correlates the radius of fluid

437   neck as a function of parameters including flow rate ratio, viscosity ratio and radius of collection

438   tube, when the dispersed phase is not perturbed,[37]

439
$$r_j = R \left[\frac{(1+\frac{Q_{DP}\eta_{DP}}{Q_{CP}\eta_{CP}})^{0.5} - \left(1+\frac{Q_{DP}}{Q_{CP}}\right)}{\frac{\eta_{DP}}{\eta_{CP}} - 2 - \frac{Q_{DP}}{Q_{CP}}} \right]^{0.5} \tag{12}$$

440   The shear rate is defined by,

441
$$\dot{\gamma} = \frac{Q_{CP}}{\pi(R^2 - r_j^2)(R - r_j)} \tag{13}$$

442   The thinning of fluid neck occurs when it is stretched and elongated at high Ca_{out}. Thus, the

443   shear rate of the continuous phase (i.e., CMC in our case) starts to decrease, and the viscosity of

444   continuous phase will increase for a shear-thinning fluid. As a result, the droplet size will start to

445   be reduced beyond a critical Ca_{out},as shown in Fig.12 when We_{in}=0.206. When the inner radius

446   of the collection tube is 0.3 mm, the droplet size increases from 0.40 mm to 0.55 mm as Ca_{out} is

447   increased from 1.5×10^{-4} to 0.0053, while the droplet size is reduced to 0.38 mm when Ca_{out} is

448   further increased to 0.015. At a given Weber number, the droplet size first increases below a

449   certain critical Capillary number due to the reduced viscosity, and then decreases above the

450   critical Capillary number, when the viscosity starts to increase again. The correlation between

451   the droplet size and the Capillary number in the Newtonian/shear-thinning two-phase system is

452   different from that in the Newtonian/Newtonian two-phase system, which normally shows that

453   droplet size scales inversely with the Capillary number of the continuous phase in a monotonous

454   fashion.[38]The different correlation highlights the complex viscosity effect towards the control

455   over emulsion droplets generated with fluid-fluid systems involving shear-thinning non-

456   Newtonian fluids. This understanding can provide information needed for designing

457   microdevicesfor generating droplets with well-defined volumes when shear-thinning non-

458   Newtonian multiphase systems are involved. For example, given certain flow conditions and

459   fluid properties (thus We_{in} and Ca_{out} are known), an analysis can be made to determine the size of

460   collection tube of the microdevice, according to the expected size of droplets in demand.
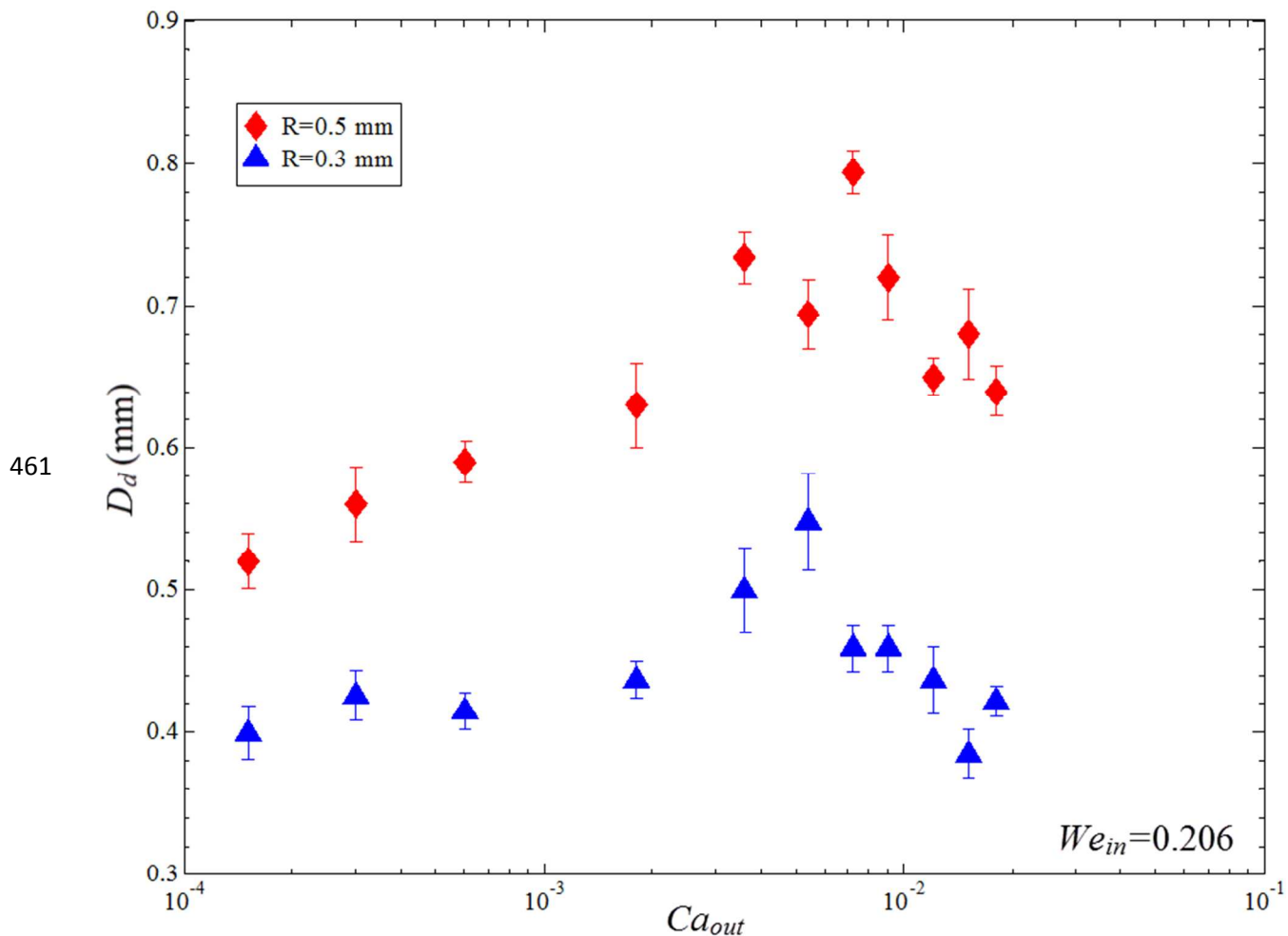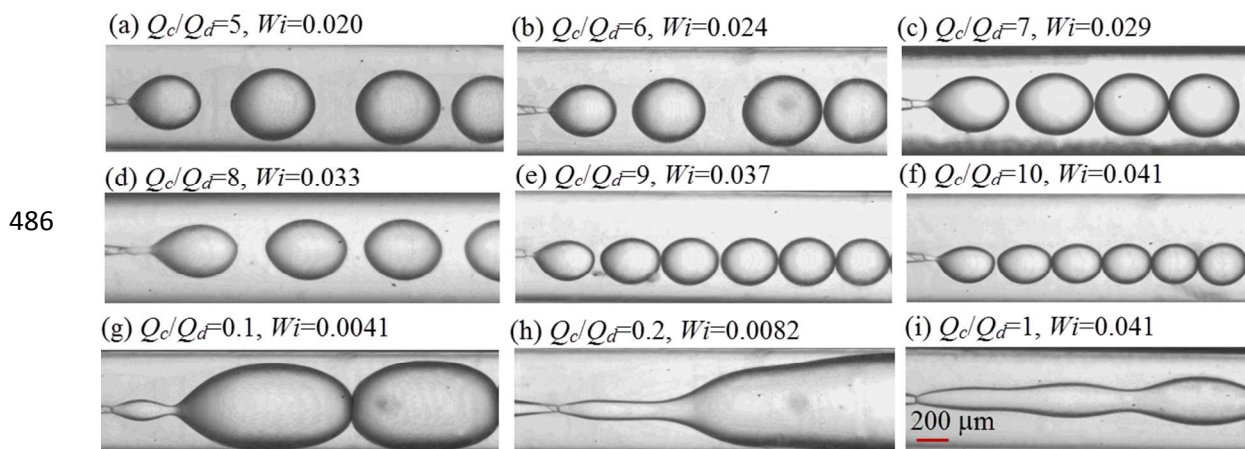
462   **Fig.12** Experimental result of droplet size as a function of the Capillary number for a given

463   collection tube in a Newtonian/shear-thinning two-phase system (silicon oil as dispersed phase

464   and CMC solution as continuous phase). We_{in}=0.206.

465   When a Newtonian liquid is surrounded by a shear-thinning liquid with pronounced elastic

466   property, the droplet breakup dynamics gets modified. We observe flow patterns at different

467   ratios of flow rate of 5% w/v PAA solution, which is the viscoelastic continuous phase, to that of

468   silicon oil as dispersed phase, as shown in Fig.13. The flow rate of dispersed phase is fixed at 1

469   ml/h in Fig.13a-f, and 10 ml/h in Fig.13g-i. The elastic forces from viscoelastic continuous phase

470   can help to overcome interfacial tension, and thus facilitate transition to jetting at smaller

471   magnitudes of the viscous forces. Compared to the aforementioned Newtonian/Newtonian or

472   Newtonian/shear-thinning multiphase microsystem where droplets normally adopt a spherical or

473   nearly spherical shape, the droplets experience significant deformation in the viscoelastic non-

474   Newtonian continuous phase. For instance, the droplets adopt an elliptical shape after breakup

475   and relax into pointed shapes. Droplets become more pointed as the radius decreases and the

476   flow rate ratio increases before it transitions to the jetting regime (see Fig.13a-f). The degree of

477   droplet deformation has been characterized based on Taylor's analysis,[39]

478
$$D_f = \frac{L-W}{L+W} \qquad (14)$$

479   where L is the half-length and W the half-breadth of the droplet. D_f increases with increasing

480   Weissenberg number (thus more pronounced elastic effect), leading to formation of droplets with

481   more pointed shape, as shown in Fig.14. This observation is consistent with the previous finding

482   that elasticity of the suspending liquid can facilitate the deformation of the Newtonian

483   droplets.[40]Our work provides a platform which will help to facilitate understanding of the

484   complex rheology behavior of viscoelastic fluid and how this behavior can affect the breakup

485   dynamics and droplet formation in multiphase microfluidic system.

486

(a) Q_c/Q_d=5, Wi=0.020   (b) Q_c/Q_d=6, Wi=0.024   (c) Q_c/Q_d=7, Wi=0.029

(d) Q_c/Q_d=8, Wi=0.033   (e) Q_c/Q_d=9, Wi=0.037   (f) Q_c/Q_d=10, Wi=0.041

(g) Q_c/Q_d=0.1, Wi=0.0041   (h) Q_c/Q_d=0.2, Wi=0.0082   (i) Q_c/Q_d=1, Wi=0.041

200 µm

487   **Fig.13** Flow patterns at selected flow rate ratios of continuous phase over dispersed phase in a

488   Newtonian/elastic-shear-thinning two-phase system (silicon oil as dispersed phase and PAA

489   solution as continuous phase). Q_d=1 ml/h for (a)-(f), and Q_d=10 ml/h for (g)-(i).

490
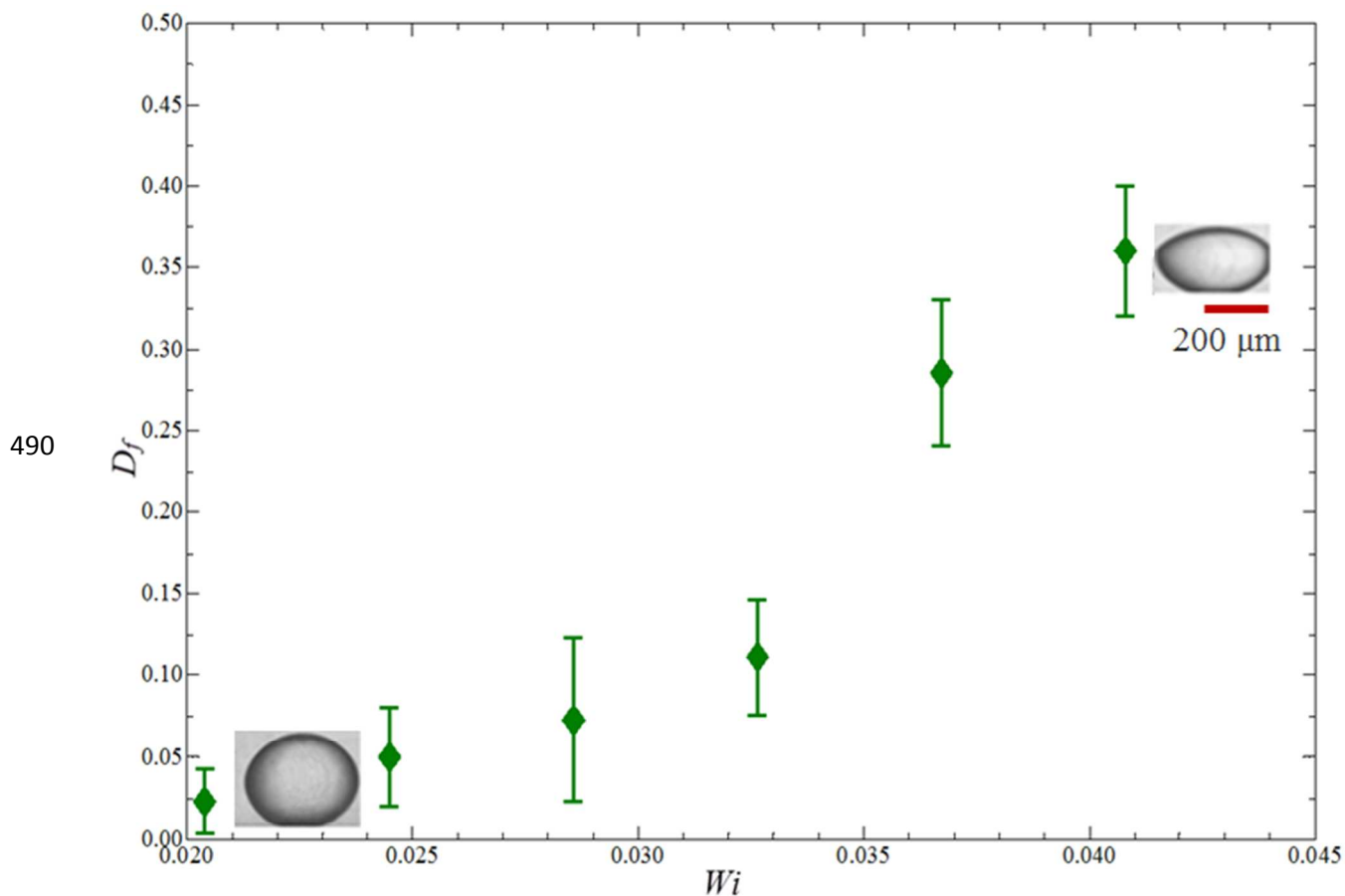
491   **Fig.14** Degree of deformation of droplet as a function of the Weissenberg number in a

492   Newtonian/elastic-shear-thinning two-phase system (silicon oil as dispersed phase and PAA

493   solution as continuous phase). The inset images show droplet adopts nearly spherical shape at

494   low Wi, while pointed shape at high Wi, respectively. The scale bar applies for both inset images.

495

496   # 5. Conclusions

497   The work reports investigation of emulsion formation using a Newtonian/shear-thinning two-

498   phase microsystem. With a shear-thinning continuous phase, the droplet dynamics is

499   characterized to predict the dripping-to-jetting transitions under different flow conditions (as

500   function of Weber number and Capillary number), where undesirable satellite droplets may be

501   formed. Inertial effects have been shown to be important for inducing the formation of a satellite

502   droplet, while the droplet formation can be suppressed by increasing viscous effect. Due to the

503   shear-thinning characteristics of the continuous phase used in the present study, the viscosity is

504   dramatically reduced at the interface; viscous effect is therefore attenuated, leading to a faster

505   breakup and a larger droplet size. Emulsions generated with non-Newtonian fluids are routinely

506   involved in drug delivery and other biochemical applications. Accurate dosing must be ensured

507   for reliable operation, and this requires excellent control over the droplet size.We also identify

508   the correlation between the droplet size and Capillary number, potentially enabling a higher

509   degree of control over the size of emulsion droplet generated with shear-thinningfluids. Finally, a

510   viscoelastic fluid is used as continuous non-Newtonian phase, and the degree of Newtonian

511   droplet deformation increases with increasing Weissenberg number of suspending non-

512   Newtonian fluid, indicating the important impact of elasticity on the droplet shape. Our work

513   provides a first framework for understanding a range of behaviors in non-Newtonian multiphase

514   microsystems, although we recognize the vast variety of non-Newtonian fluids besides the two

515   types (shear-thinning solution with or without elastic property) we have investigated and the

516   large regions of unexplored operating conditions. For example, it is challenging to generate

517   droplets with non-Newtonian fluids in aqueous two phase systems (ATPS) due to much lower

518   interfacial tension when compared with oil-water systems.[41-42]Furthermore, it is also of great

519   interest to investigate the cases when non-Newtonian fluid is used as the dispersed phase, rather

520 than just the continuous phase. Improvement in the polydispersity of the resultant droplets can

521 also be achieved potentially by developing and implementing methods to dynamically control the

522 merging of satellite droplets with the main droplets. This approach of elimination of satellite

523 droplets will also lead to droplets with higher size uniformity in applications that inevitably

524 involve non-Newtonian multiphase flows.

525 ## Acknowledgement

533 ## Reference

534 1 H.C. Shum, D. Lee, I. Yoon, T. Kodger and D.A. Weitz, *Langmuir*, 2008, **24**, 7651–7653.

535 2 T. Kong, J. Wu, M.To, K.W.K. Yeung and H.C. Shum, *Biomicrofluidics*, 2012, **6**, 034104.

536 3 C.I. Zoldesi, P. Steegstra and A. Imhof, *J. Colloid Interface Sci.*, 2007, **308**, 121–129.

537 4 J.K. Nunes, S.S.H. Tsai, J. Wan and H.A. Stone, *J. Phys. D Appl. Phys.*, 2013, **46**, 114002.

538 5 C.H. Choi, H. Yi, S. Hwang, D.A. Weitz and C. Lee, *Lab Chip*, 2011, **11**, 1477.

539 6 C.M. Hwang, A. Khademhosseini, Y. Park, K. Sun and S. Lee, *Langmuir*, 2008, **24**, 6845–
540   6851.

541 7 J.Wu, T. Kong, K.W.K.Yeung, H.C. Shum, K.M.C. Cheung, L. Wang, and M.K.T. To, *Acta*
542   *Biomaterialia*, 2013,**9**(7), 7410-7419.

543 8 Ö.E. Yıldırım and O.A. Basaran, *J. Non-Newtonian Fluid Mech.*, 2006, **136**, 17–37.

544 9 A.R. Abate, M. Kutsovsky, S. Seiffert, M. Windbergs, L.F.V. Pinto, A.Rotem, A.S. Utada and
545   D.A. Weitz, *Adv. Mater.*, 2011, **23**, 1757–1760.

546 10 C. L. A. Berli, *J. Colloid Interface Sci.*, 2010, **349**, 446–448.

547 11 T. Nguyen, Y. Xie, L. J. de Vreede, A. van den Berg and J.C.T. Eijkel, *16th Int. Conf. on*
548   *Miniaturized Systems for Chemistry and Life Sciences*, 2012, 1987–1989.

549 12 D.J. Mcclements, *Crit. Rev. Food Sci.Nutr.*, 2007, **47**, 611–649.

550 13 A. Budhian, S.J. Siegel and K.I. Winey, *Int. J. Pharm.*, 2007, **336**, 367–75.

551 14 C. Berkland, M. King, A. Cox, K. Kim and D. Pack, *J. Control Release*, 2002, **82**, 137–47.

552 15 R.M. Erb, D. Obrist, P.W. Chen, J. Studer and A.R. Studart, *Soft Matter*, 2011, **7**, 8757.

553 16 M.S.N. Oliveira and G.H. McKinley, *Phys. Fluids*,2005, **17**,071704.

554 17 J. Eggers1 and E. Villermaux, *Rep. Prog. Phys.*, 2008, **71**,036601.

555 18 A.S. Utada, A. Fernandez-Nieves, H.A. Stone and D.A. Weitz, *Phys. Rev. Lett.*, 2007, **99**,
556   094502.

557 19 R.G.Larson, *Thestructure and rheology of complex fluids*, Oxford University Press, Oxford,
558   1999.

559 20 S.Yang, J.Y.Kim, S.J.Lee, S.S. Lee, and J.M.Kim, *Lab Chip*, 2011, **11**, 266.

560 21 L.Derzsi, M.Kasprzyk, J.P.Plog, and P.Garstecki, *Phys. Fluids*, 2013,**25**, 092001.

561 22 G. Pangalos, J.M. Dealy and M.B. Lyne, *J. Rheol.*,1985, 29, 471–491.

562 23 A. Sauret, C. Spandagos and H.C. Shum, *Lab Chip*, 2012, **12**, 3380.

563 24 L.Sang, Y.Hong and F. Wang, *Microfluid Nanofluid*, 2009,**6**, 621–635.

564 25 C.L. Tucker, *Hanser Publishers*, New York, 1989.

565 26 Y. Hong and F. Wang, *Microfluid Nanofluid*, 2007, **3**,341–346.

566 27 A. Benchabane and K. Bekkour, *Colloid. Polym. Sci.*, 2008, **286** (10), 1173-1180.

567 28 K. Benyounes, *13th SGEM GeoConference on Science and Technologies In Geology,*
568 *Exploration and Mining*, 2013, 951–95.

569 29 S.D. Geschiere, I.Ziemecka, V. van Steijn, G.J.M. Koper, J.H. van Esch and M.T. Kreutzer,
570 *Biomicrofluidics*, 2012,**6**, 022007.

571 30 A. Kreiba, *The Rheological Properties of Aqueous Polyacrylamide Solutions*, Concordia
572 University, 2000.

573 31 R. G. Larson, *Constitutive Equation for Polymer Melts and Solutions*, Butterworth-
574 Heinemann, 1988.

575 32 J. Eggers, *ZAMM · Z. Angew.Math. Mech.*, 2005, **85**,400–410.

576 33 M.Rohani, F.Jabbari and D. Dunn-Rankin, *Phys. Fluids*, 2010, **22**, 107103.

577 34 M. Tjahjadi, H.A. Stone and J. M. Ottino, *J. Fluid Mech.*,1992, **243**,297–317.

578 35 G.I. Taylor, *Proc. R. Soc.LondonSer.A*, 1932, **138**, 41–47.

579 36 H. Song, D.L. Chen and R.F.Ismagilov, *Angew. Chem. Int. Ed.*, 2006, **45**, 7336–7356.

580 37 A. Sauret and H.C. Shum, *Int.J.Nonlin. Sci. Num.*, 2012, **13**, 351-362.

581 38 C.A. Stan, S.K.Y. Tang and G.M. Whitesides, *Anal. Chem.*, 2009, **81**, 2399–2402.

582 39 G.I. Taylor, *Proc. Roy.Soc.A*, 146 (1934) **501**.

583 40 D.C. Tretheway and L.G. Leal, *J. Non-Newtonian Fluid Mech.*, 2001, **99**, 81–108.

584 41 Y.Song, A. Sauret and H.C. Shum, *Biomicrofluidics,* 2013,**7**, 061301.

585   42 A.Sauret and H.C. Shum, *Appl. Phys. Lett.,*2013, **100**, 154106.

38